Mass Transfer under Bubble-Induced Convection in a Vertical Electrochemical Cell

Atul Shah*,[1]

Department of Chemical Engineering, Wayne State University, Detroit, Michigan 48202

Jacob Jorne*

Department of Chemical Engineering, University of Rochester, Rochester, New York 14627

ABSTRACT

Mass transfer under bubble-induced convection has been experimentally measured in a vertical cell. The cell consisted of two parallel vertical electrodes, upon one of which chlorine gas evolved and the other where the mass-transfer-controlled reduction of dissolved chlorine occurred. Two mechanisms contributed to the enhancement of mass transfer: circulation due to the nonuniform distribution of bubbles and stirring caused by the rising bubbles. The average mass-transfer coefficient generally decreased with increasing cell gap, except at a cell gap of about 0.5 cm where a local maximum occurred. The local mass-transfer coefficient increased nonlinearly with height. A mathematical model for the bubble-driven fluid flow in the electrochemical cell is presented where bubble-induced convection can be treated as a natural convection phenomenon. The governing differential equations are developed and the results of the numerical analysis are presented and discussed in light of the assumed distribution of the void fraction. A qualitative agreement with observed flow patterns is obtained.

Many electrochemical reactions of commercial interest have one or more products in the gaseous phase. These products are formed on the electrode surface and released in the form of bubbles in the liquid electrolyte. Three of the most common products are hydrogen, oxygen, and chlorine. In other industrial electrochemical cells, inert gases such as nitrogen and air are sparged into the cell to stir the electrolyte. An example of such an application is the copper electrowinning cell.

The presence of gas bubbles in the electrochemical cell affects the performance of the cell in two independent ways. First, gas bubbles in the path of the electric current between the two electrodes of the cell decrease the effective conductivity of the electrolyte, which increases ohmic losses of the cell. Second, the buoyancy force acting on the gas bubbles induces hydrodynamic convection in the cell gap, which has a profound effect on the rate of mass transfer of species to and from the electrode surface.

The enhancement of convective mass transfer due to gas bubbles is the subject of this investigation. Often, the increased rate of mass transfer benefits the cell performance. This is not true in all cases, as in the case of the zinc-chlorine battery, where the mass transfer of dissolved chlorine across the cell gap is undesirable.

Two types of mass-transfer enhancement due to gas evolution can be distinguished: (*i*) gas evolving electrodes where the gas evolution and the mass transfer occurs at the same electrode, and (*ii*) external gas introduction where gas bubbles are introduced physically or electrochemically in order to enhance mass transfer in the electrochemical cell. Gas bubbles can be introduced by gas sparging in the cell gap or by electrochemically evolving gas bubbles at an electrode placed near the electrode where mass-transfer enhancement is desirable. In most cases, gas evolution at the counterelectrode can serve this purpose.

The present investigation is concerned with the case where the mass transfer at a vertical electrode is affected by the close proximity of a vertical gas evolving electrode. The mass transfer of dissolved chlorine is measured at a vertical electrode while chlorine gas is evolved at a nearby vertical electrode. The effects of spacing and cell geometry on the mass transfer are investigated and discussed.

The published research on mass transfer due to bubble-driven circulation can be classified into two categories. The first category deals with mass transfer to a gas evolving electrode (1-6). The studies under this category concentrate on the mass transfer at the same electrode surface on which gas bubbles are formed and released. The second category involves the investigation of mass transfer at a gas-sparged electrode (7-14). This category includes cases where gas is introduced externally through a sparger placed in the cell gap and gas evolves electrochemically at one electrode, and the mass transfer to the other electrode is the subject of investigation. It is clear that there is a significant difference in the mechanism of mass transfer in the two categories mentioned above. The present investigation deals with the second category where gas evolves electrochemically at one electrode and the mass transfer to the other electrode is affected.

Gendron and Ettel (7) compared the enhancement in the mass-transfer coefficient caused by three different modes of convection during copper electrodeposition: the forced recirculation of electrolyte in a direction parallel to a copper cathode, oxygen gas evolution on the anode, and air sparging over the face of the cathode. Their experimental technique included measurement of limiting current for codeposition of silver with copper (8). They concluded that air sparging in the cell gap is a better method for mass-transfer enhancement because it results in a uniform mass transfer over the cathode surface. A high local mass-transfer coefficient was measured at the top, compared to the local mass-transfer coefficient at the bottom where laminar natural convection dominates. Mohanta and Fahidy (9) investigated the enhancing effect of gas bubbles generated at an anode on the ionic mass transfer at the associated cathode. Their experimental system included a laboratory-scale copper electrowinning cell with copper cathode and an anode on which oxygen gas evolved. They noted that at higher cell gaps, a smaller portion of the bubbles travels across the cell gap toward the cathode and hence the enhancement of the mass-transfer coefficient is smaller. For the taller electrode, a larger fraction of the total cathode area is affected by bubble driven convection; hence, the enhancement in the mass-transfer coefficient is higher. Sedahmed (10) investigated the enhancement of the mass-transfer coefficient for copper deposition on a vertical cylinder cathode stirred by oxygen evolved on a lead anode placed below the cylinder. Sedahmed and Schemilt (11) measured the mass-transfer coefficient for the deposition of copper at a vertical-plate cathode placed in copper sulfate electrolyte stirred by oxygen evolved at a coplanar vertical-plate lead electrode positioned upstream from the cathode. It is reported (11) that the flow turns from laminar to turbulent above a certain electrode height. The bubbles in the swarm interact among each other to affect the rising velocity in two different ways. A chimney ef-

*Electrochemical Society Active Member.
[1]Present address: Teledyne Analytical Instruments, City of Industry, California 91748.

Downloaded on 2015-06-09 to IP 141.210.2.78 address. Redistribution subject to ECS terms of use (see ecsdl.org/site/terms_use) unless CC License in place (see abstract).

fect can develop in which massive upward flow at the axis of the swarm leads to increased net bubble velocity and the proximity of the bubbles to one another can result in a hindered settling condition leading to reduced average bubble velocity.

Sigrist *et al.* (12) investigated mass transfer at a vertical gas-sparged electrode with and without superimposed electrolyte flow for three different cell configurations. The electrolytic gas evolution was simulated by a vertical porous plate through which the gas entered the cell. It was observed that the distance between the electrodes has no influence on the rate of mass transfer and the mass-transfer rate decreases with increasing the superimposed liquid flow. They proposed the following explanation for the decrease: the superimposed liquid flow causes the rising velocity of the bubbles to increase which in turn results in an expansion of the bubble swarm and a corresponding decrease of void fraction. They also observed that the mass-transfer rate is a function of void fraction, irrespective of the values of liquid and gas flow rates. From the proceeding observations, Sigrist *et al.* (12) deduced that the macroscopic flow situation is not a relevant factor in mass transfer from a dispersed system to a solid wall. The increase in mass transfer with the void fraction suggests that the motion of individual bubbles plays an important role. They proposed the following correlation for the mass transfer rate

$$\mathrm{Sh} = 0.19\,(\mathrm{Sc}\,\mathrm{Ar}^*)^{0.33} \qquad [1]$$

where Sh is the Sherwood number, Sc is the Schmidt number, and Ar* is a modified Archimedes number $gd^3\epsilon\nu^{-2}(1-\epsilon)^{-1}$. This correlation is identical to the one for mass and heat transfer under turbulent natural convection conditions. It implies that the mass-transfer rate does not depend on the height of the electrodes and the distance between them.

Ibl (13) presented a model that allows a theoretical interpretation of the similiarities between mass transfer at vertical gas sparged electrodes and turbulent natural convection. The correlation proposed by Ibl (13) is similar to the one given by Sigrist *et al.* (12) except that the Sh is replaced by $\mathrm{Sh_d}$, a Sherwood number based on the cell gap (d). In this model, the macroscopic vortices of the two phase system (gas and liquid) are considered to have a major effect on the mass-transfer rate. This is unlike the model proposed by Sigrist *et al.* (12) in which the eddies formed in the wake of individual bubbles are considered to have a major effect on the mass-transfer rate. The system is considered turbulent near the top of the electrode for which the proposed correlation holds. The presence of a macroscopic vortex at the top of the cell is reported by Ibl (13). It is also observed that the bubble envelope of the lower part of the cell suddenly broadens at a certain height where it abruptly expands across the cell gap and reaches the opposing electrode. The height at which the bubble envelope broadens depends on the height of the liquid above the upper edge of the working electrode, the free surface available for bubble detachment and its kinetics.

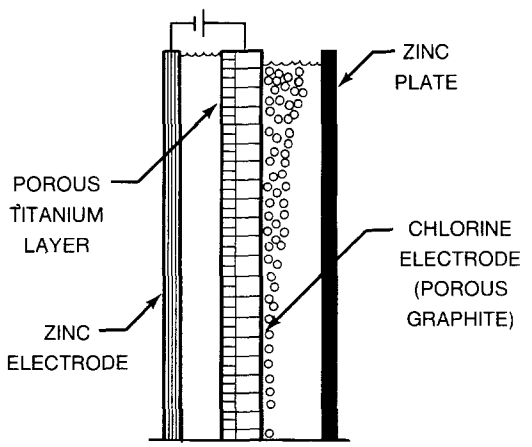

Fig. 1. Experimental determination of isolated effect of bubble-induced convection using weight loss measurements.

Mass transfer to a vertical electrode under gas sparging was investigated recently by Cavatorta and Böhm (14). It was found that the enhancing effect of gas bubbles is a function of the gas hold-up ϵ, irrespective of the gas flow and gas distributor employed. A correlation for fully developed mass transfer has been obtained

$$\mathrm{Sh} = 0.256\,(\mathrm{GaSc})^{1/3}\,\epsilon^{0.254} \qquad [2]$$

This correlation is similar in form to the correlation for turbulent mass transfer under natural convection, except the Galileo number $\mathrm{Ga} = L^3 g\nu^{-2}$, the Schmidt number $\mathrm{Sc} = \nu/D$, and the gas hold-up ϵ are the relevent dimensionless parameters.

The flow regime of liquid circulation due to gas evolution has been theoretically investigated by Ziegler and Evans (15) for electrowinning cells, using turbulence and bubble turbulent diffusion. They favorably compared their predictions to their measurements and the experimental mass-transfer results of Ettel *et al.* (8).

Experimental

The effect of bubble-induced convection on mass transfer was investigated by electrochemically evolving chlorine gas from $ZnCl_2$ solution on a vertical porous electrode and by measuring the mass-transfer rate for its reduction at another electrode located parallel to the gas evolving electrode.

In order to isolate the bubble-induced convection, a porous graphite electrode is plasma-sprayed with porous titanium on the side facing a zinc counterelectrode. This forces the chlorine gas evolution on the noncoated side of the porous graphite electrode. A dense graphite or a zinc plate is placed at an appropriate gap facing the chlorine evolving side of the porous graphite plate. In this fashion, the bubble-induced convection is isolated from the forced and natural convections occurring at the counter zinc electrode. Nonetheless, a very weak natural convection, caused by $ZnCl_2$ formation, occurs at the measuring electrode.

The local and average mass-transfer coefficients of dissolved chlorine due to bubble-induced convection alone were determined by two methods: (*i*) By measuring the weight losses of the zinc plate caused by the corrosion reaction

$$\mathrm{Zn(s) + Cl_2(aq) \rightarrow ZnCl_2(aq)}$$

which has been shown to be mass-transfer limited (16). (*ii*) By measuring the limiting currents for chlorine reduction at a dense graphite plate exposed to chlorinated electrolyte in which chlorine bubbles evolved electrochemically. The reaction is

$$\mathrm{Cl_2(aq) + 2e^- \rightarrow 2\,Cl^-(aq)}$$

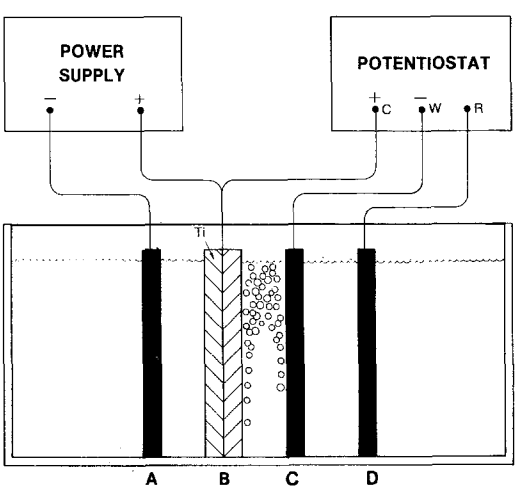

Fig. 2. Experimental setup for limiting current measurements. A, Auxiliary electrode: dense graphite. B, Gas-evolving electrode: titanium-sprayed porous graphite. C, Working electrode: dense graphite. D, Reference electrode: porous graphite, Cl_2/Cl^-.

Downloaded on 2015-06-09 to IP 141.210.2.78 address. Redistribution subject to ECS terms of use (see ecsdl.org/site/terms_use) unless CC License in place (see abstract).

In both cases, 10 × 10 cm porous graphite (Union Carbide PG-60) electrode, plasma sprayed with titanium on one side was used as the chlorine evolving electrode. The experimental setup of the weight loss measurements is shown in Fig. 1. In some experiments, segmented zinc plate, made of horizontal strips, was used in order to measure the local distribution of the corrosion reaction.

The experimental setup for the limiting current experiments is shown in Fig. 2. Chlorine gas was evolved by passing constant current between the gas evolving electrode and the auxiliary zinc electrode. The dense graphite electrode, on which the limiting current is being measured, was held at potentials where zinc deposition does not take place. The chlorine reduction limiting current was measured by a shunt. The Cl_2/Cl^- reference electrode consisted of a porous graphite electrode submerged in the same electrolyte.

The local limiting currents for chlorine reduction were measured on five small graphite probes (6.35 mm diam) which were inserted into the graphite plate and insulated by Kynar heat shrinking sleeves. The current on each probe was measured by a low resistance shunt and the potentials of the probes were always maintained at the potential of the plate in which they were embedded. This was achieved by an operational amplifier circuit shown in Fig. 3.

All experiments were carried out in chlorinated 1.5*M* $ZnCl_2$ solution at 22°-25°C. The chlorine solubility was about 2.5 g/liter and the rate of chlorine bubble evolution corresponded to a current density of 33 mA/cm^2. The mass-transfer coefficients for dissolved chlorine were calculated from the measured limiting current densities according to

$$k = \frac{i_l}{n\mathbf{F}[Cl_2]} \qquad [3]$$

where i_l is the limiting current density, $n = 2$ is the number of electrons transferred, and $[Cl_2]$ is the solubility of dissolved chlorine in the electrolyte. Further details of the experimental procedure are given elsewhere (17-19).

Results

The effect of cell gap on the average mass-transfer coefficient is shown in Fig. 4. The curve can be divided into three sections: (*i*) For the cell gap 0-4 mm the mass-transfer coefficient decreases with increasing cell gap, because the fluid motion, induced by the rising chlorine bubbles, becomes less intense; (*ii*) In the cell-gap range of 4-5 mm the mass-transfer coefficient increases. One possible explanation is that in this range a well-defined return flow is established which does not interfere with the rising bubbles; and (*iii*) For the cell gaps beyond 5 mm, the mass-transfer coefficient decreases with increasing cell gap and is expected to attain a steady value at larger cell gaps which corresponds to the contribution due to natural convection in infinite medium. In all regimes there is a return flow; however, in the thin gap regime the downcoming flow is less significant and the fluid percolates through the rising bubbles, while in the thick gap regime, a spatially separated downcoming flow is well established. It can be noticed in Fig. 4 that the general behavior of the two curves, obtained by two independent methods, is similar. However, the values of the mass-transfer coefficients obtained by the limiting current method are higher by 10-20% than those obtained by the zinc corrosion method. This difference can be due to the roughness of the dense graphite compared to the zinc plate. Figure 5 shows a representation of visual observations of the fluid motion for a cell gap of 5 mm. Higher convection occurs at the top of the cell where a vortex can be observed due to the circulation of the mixture of electrolyte and gas bubbles. For smaller cell gaps the return flow is opposed by the rising bubbles.

The height distribution of the local mass-transfer coefficient is shown in Fig. 6. These data were obtained using segmented zinc plates and potentiostatic limiting current on probe electrodes. The local mass-transfer coefficient increases with distance from the bottom of the electrode. The increase is due to the accumulation of rising bubbles which causes more intense fluid motion. The local mass-transfer coefficients for the lower half decrease with increasing the cell gap. However, for cell gaps beyond 3 mm, the mass-transfer coefficients for the upper half increase with cell gap. The increase in average mass-transfer coefficient from 4 to 5 mm cell gap is due to the increase in local mass-transfer coefficients for the upper half of the zinc plate. Figure 4 shows the zinc corrosion measurement to be lower than the potentiostatic, but Fig. 6, in which local distribution is reported, shows the reverse trend. It is possible that the segmented zinc electrode is responsible for the higher local mass transfer rates.

The shape of the bubble envelope formed near vertical gas evolving electrodes is shown schematically in Fig. 7 where two distinct shapes of expanding envelopes of gas bubbles can be seen. The bubble envelope expands with height due to the accumulation of gas bubbles. In the case of smaller cell gaps, the bubble envelope expands almost linearly with height and reaches the opposing wall gradually as shown in Fig. 7a. A weak circulation loop is established in the bottom section of cell gap. The velocity of the liquid does not significantly affect the shape of the bubble envelope. For larger cell gaps, the bubble envelope expands linearly with height near the bottom of the cell. The circulation loop is taller and stronger than in the case of the

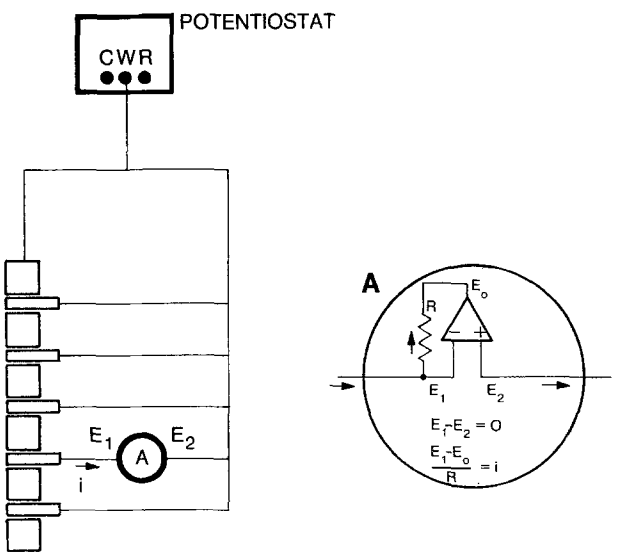

Fig. 3. Circuit for maintaining equal potential on probe

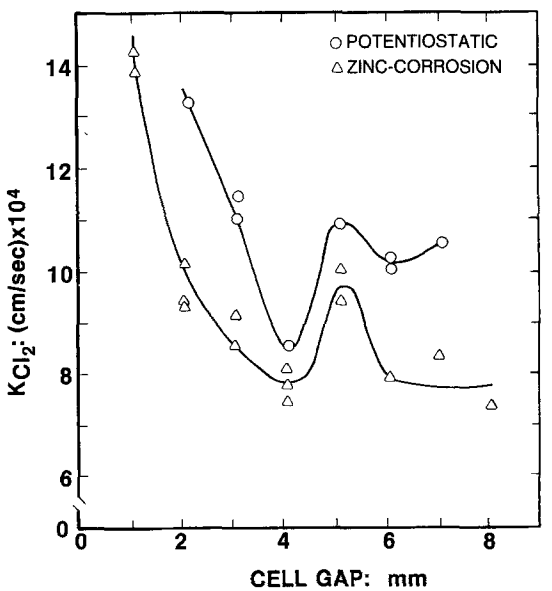

Fig. 4. Bubble-induced convection: mass-transfer coefficient vs. cell gap.

Downloaded on 2015-06-09 to IP 141.210.2.78 address. Redistribution subject to ECS terms of use (see ecsdl.org/site/terms_use) unless CC License in place (see abstract).

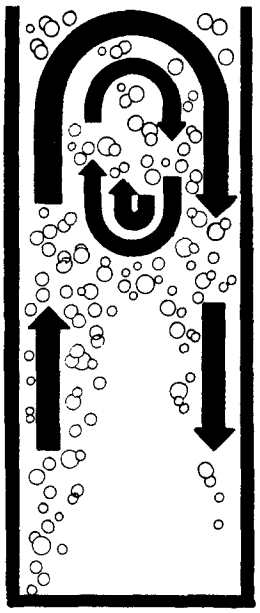

Fig. 5. Representation of the vortex near the top of electrode in bubble-induced convection at a cell gap of 5 mm.

smaller cell gap. The liquid velocity affects the shape of the bubble envelope. In the upper section, the envelope expands abruptly and reaches the opposing wall as shown in Fig. 7b. The abrupt expansion of the bubble envelope is due to the horizontal component of the liquid velocity toward the opposing wall. The horizontal velocity near the bottom is toward the gas evolving wall, and hence the bubble envelope is narrower than in the case of smaller cell gaps. For smaller cell gaps, the bubble envelope gradually

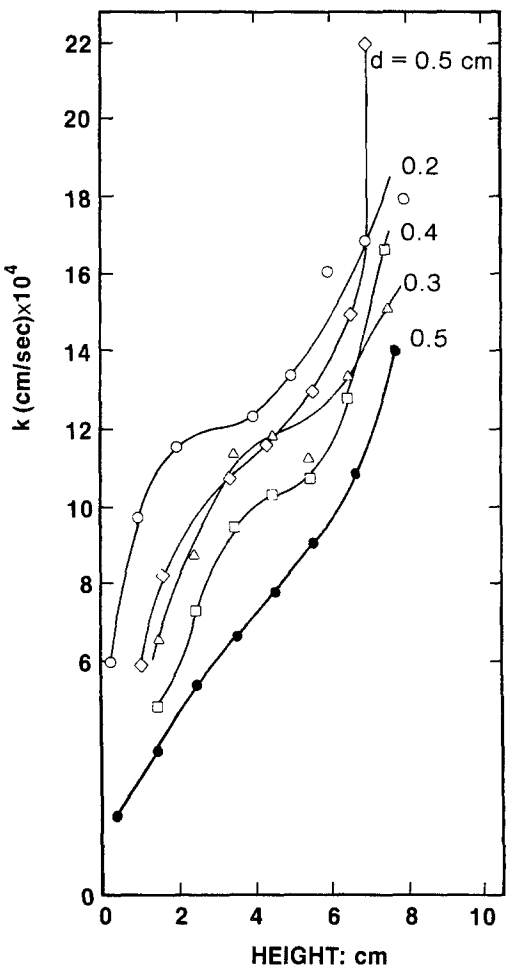

Fig. 6. Local mass-transfer coefficients vs. height obtained by weight loss measurements of segmented zinc plate and potentiostatic measurements (bold circles).

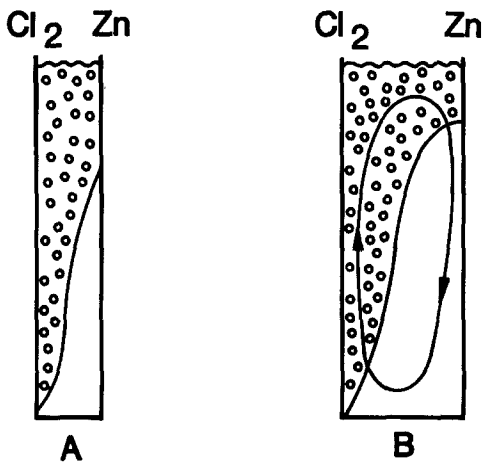

Fig. 7. Schematic representation of region in which gas bubbles are confined.

reaches the opposing wall before the horizontal component of the liquid velocity can become strong enough to drag the bubbles along. It is easy to see that in the case of a larger cell gap, a well-defined circulation loop occupies most of the cell gap. The critical cell gap at which the liquid velocity begins to affect the shape of bubble envelope is expected to be a function of the rate of gas evolution on the vertical electrode. The data reported here were collected at current density of 33 mA/cm^2, which corresponds to a rate of chlorine gas evolution of 0.251 cm^3/cm^2-min.

Discussion

An attempt is made here to analyze and explain the experimental results for isolated bubble-induced convection. It is believed that in the case of mass transfer to a vertical gas-sparged electrode the following two mechanisms contribute to the overall rate of mass transfer:

1. The mass transfer due to the stirring or disturbance caused by the rising bubbles.
2. The mass transfer due to the well-defined circulation of liquid caused by the variable density.

The contribution to overall mass transfer due to the disturbance caused by the rising bubbles would exist even if the bubbles were uniformly distributed in the liquid. However, the well-defined circulation loop, similar to one in the case of natural convection caused by a temperature gradient, would occur only if the bubbles were distributed nonuniformly, causing density gradient in the horizontal direction. In the case of a bubble column, where the gas bubbles are introduced uniformly at the bottom, the mass transfer to the vertical walls occurs only due to the disturbance caused by the rising bubbles and the well-defined circulation loop does not exist. The downcoming liquid percolates back through the rising bubbles. On the other hand, in the case of natural convection due to temperature or concentration gradient, the mass transfer to vertical walls occur only due to circulation of liquid. The identification of a thin gap regime where the downcoming flow is less significant and a thick gap regime where the downcoming is spatially established has not been reported before. Sigrist *et al.* (12) did not observe cell gap dependency as can be seen from Eq. [1]. The transition in the present work occurs at 4 mm, however, it is expected to depend on the electrode height.

We do not have experimental data on the rate of mass transfer due to the individual mechanisms. The mass transfer due to the disturbance caused by rising bubbles is expected to depend on the proximity of bubbles to the vertical wall and the velocity of the bubbles. As the cell gap is increased, most of the bubbles would not reach the cathode and the contribution to the overall mass transfer due to this mechanism would decrease. As shown in Fig. 7, due to the accumulation with height, bubbles come close to the vertical cathode in the top section of the cell. Hence, the contribution to local mass transfer, due to disturbance caused by the rising bubbles would increase along the height of the electrode.

Downloaded on 2015-06-09 to IP 141.210.2.78 address. Redistribution subject to ECS terms of use (see ecsdl.org/site/terms_use) unless CC License in place (see abstract).

The rate of mass transfer due to the circulation of liquid depends on the gradient of velocity at the vertical cathode. A hydrodynamic model for the circulation caused by the density gradient in the horizontal direction is presented by Shah (17), and the results of the model will be discussed later in the theoretical section. For small cell gaps, contrary to our expectation, the velocity of the circulation loop increases with an increase in the cell gap. This is due to the decrease in the viscous losses. The higher velocity results in a steeper gradient at the vertical cathode and hence, the contribution to the overall mass transfer, due to the circulation of liquid, increases with an increase in the cell gap. However, the velocity of liquid circulation cannot keep increasing with cell gap in the entire range of cell gaps. At a definite cell gap, the velocity of the circulation loop would reach a maximum and then decrease with an increase in the cell gap. This would cause a decrease in the rate of mass transfer. A higher rate of local mass transfer near the top of the cathode is suggested by the intense circulation in the top region.

The contribution due to the individual mechanisms and the combined mass-transfer coefficient are qualitatively shown in Fig. 8. The curve for the combined mass-transfer coefficient is similar to the experimental curves in Fig. 4 and only qualitative agreement is observed.

The general shape of the experimental curves presented in Fig. 4 and 6 does not entirely agree with the experimental data published by other investigators (7, 9-12). The major reason for this apparent disagreement is the unique geometry of the experimental cell used in this investigation. Some important differences are discussed below. (*i*) The cell gaps investigated here are smaller than those investigated by others. In this study the cell gap was varied from 0.1 to 0.8 cm. In most other published investigations the cell gaps range from 1.0 to 5.0 cm. (*ii*) The cavity between the two electrodes is closed at the bottom. This prevents the circulation of liquid around either electrode and includes a circulation loop within the cavity. (*iii*) The rate of gas evolution of 0.25 cm^3/cm^2-min, is lower than the rates used by other investigators. (*iv*) The mass-transfer coefficient is measured along the entire surface of a 10 cm tall electrode, unlike Sigrist *et al.* (12) who measured the rate of mass transfer only for a small section at the top.

Theoretical Analysis

The theoretical analysis is divided into two sections: mass transfer under bubble-induced convection and bubble-driven fluid flow in a vertical electrochemical cell.

Mass transfer under bubble-induced convection.—The bubble-induced mass transfer can be treated similarly to natural convection due to concentration or temperature variations (13, 20, 21). The density variation here is caused by the void fraction in the vicinity of the gas evolving electrode.

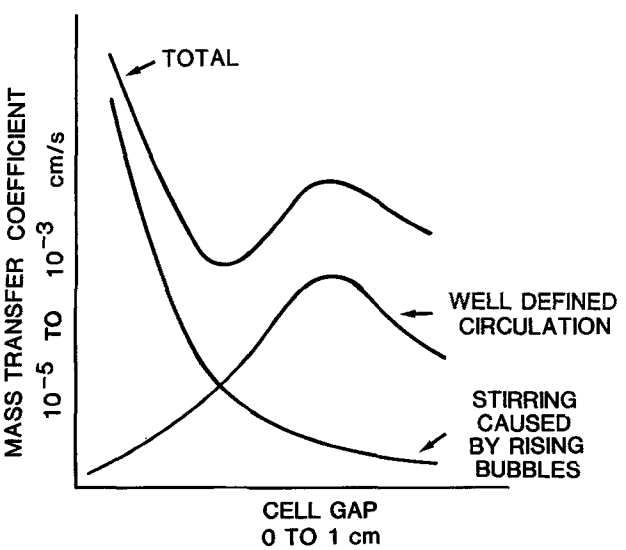

Fig. 8. Schematics of contribution by individual mechanisms

The general correlation for mass transfer under turbulent natural convection is given by

$$\mathrm{Sh} = a(\mathrm{Gr} \cdot \mathrm{Sc})^{1/3} \quad [4]$$

where a is a constant and the dimensionless numbers are based on the height of the electrode

$$\mathrm{Sh} = \frac{kh}{D} \quad [5]$$

$$\mathrm{Gr} = \frac{gh^3\epsilon}{\nu^2(1-\epsilon)} \quad [6]$$

$$\mathrm{Sc} = \nu/D \quad [7]$$

where k is the mass-transfer coefficient, D the diffusion coefficient, ν the kinematic viscosity, ϵ is the void fraction of the electrolyte-bubbles mixture, g is the gravitational acceleration, and h is the electrode height. The mass-transfer coefficient k is given by

$$k = aD^{2/3}(\nu)^{-1/3}g^{1/3}\left[\frac{\epsilon}{1-\epsilon}\right]^{1/3} \quad [8]$$

Accordingly, a logarithmic plot of k *vs.* $(\epsilon/1-\epsilon)$ should give a straight line with a 1/3 slope.

In order to estimate the void fraction, a simplified model has been used. The void fraction is defined by

$$\epsilon = \frac{V_g}{V_l + V_g} \quad [9]$$

where V_g and V_l are the volume of gas and liquid, respectively in the cell gap

$$V_l + V_g = dbh \quad [10]$$

where d, b, and h are the cell gap, width, and height, respectively.

The volume of the gas V_g can be expressed as

$$V_g = \dot{V}_g \times t \quad [11]$$

where $\dot{V}_g$ is the volume rate of gas evolution and t is the residence time. The volumetric rate of gas evolution can be obtained by Faraday's law

$$\dot{V}_g = \frac{\bar{V}_m bhi}{n\mathbf{F}} \quad [12]$$

where $\bar{V}_m$ is the molar volume of a gas under STP, and i is the applied current density.

A simplified assumption is made to determine the average residence time t. It is assumed that all the bubble uniformly rise through the entire height (h) of the electrode. Therefore

$$t = \frac{h}{2v} \quad [13]$$

where v is rising velocity of the bubbles, and hence

$$V_g = \frac{\bar{V}_m bh^2 i}{2n\mathbf{F}v} \quad [14]$$

Substituting in Eq. [9] gives

$$\epsilon = \frac{\bar{V}_m hi}{2dn\mathbf{F}v} \quad [15]$$

For the experimental conditions of h = 10 cm, i = 0.03 A/cm^2 d = 2-8 mm and an assumed constant rising velocity, it can be approximated that

$$\frac{\epsilon}{1-\epsilon} \simeq \frac{\bar{V}_m hi}{2dn\mathbf{F}v} \quad [16]$$

Downloaded on 2015-06-09 to IP 141.210.2.78 address. Redistribution subject to ECS terms of use (see ecsdl.org/site/terms_use) unless CC License in place (see abstract).

Therefore, the mass-transport coefficient is inversely proportional to the cell gap

$$k \propto \left(\frac{hi}{d}\right)^{1/3} \quad [17]$$

A logarithmic plot of the mass-transfer coefficient *vs.* the cell gap is shown in Fig. 9. An approximated slope of $-1/3$ can be observed for cell gaps up to 4 mm. Beyond this gap, the mass-transfer coefficient increases probably due to the establishment of a return flow and circulation within the cell gap, as discussed above. Thus, bubble-induced convection can be treated as a natural convection phenomenon. This convection is driven by the density variation due to the void fraction of the bubble-electrolyte mixture adjacent to the gas evolving electrode. The constant a in Eq. [4], can be estimated from Fig. 9 once the rising velocity v is known. By visual observation, the rising velocity was estimated at 1 cm/s and the constant a is approximated at $a = 0.12$, in reasonable agreement with $a = 0.31$, obtained by Fouad and Ibl (23) for turbulent natural convection at vertical electrode.

According to this model, the mass transfer coefficient depends on the electrode height to the 1/3 power and on the current density to the $-1/3$ power. These dependences have not been investigated in the present work.

Bubble-driven fluid flow in a vertical electrochemical cell.—The fluid flow due to bubble induced convection in an electrochemical cell consists of a two-phase mixture, gas and liquid, flowing in a narrow vertical channel. A large number of very small bubbles are dispersed into the continuous liquid phase. The rectangular coordinate system used for the modeling is defined in Fig. 10. The bottom left-hand corner of the rectangular cavity is selected as a coordinate origin. The components of velocity in the x and y directions are u and v, respectively. The height of the electrodes is "l" and the distance between the two electrodes is denoted by "d." The electrode on the left is the anode on which gas bubbles evolve. The wall on the right could be a metal plate or a working electrode depending on the experimental method. The bottom of the cell is closed and the top is a free surface.

The following assumptions were made while formulating the governing differential equations for the bubble-driven fluid flow in an electrochemical cell:

1. The Boussinesq approximation: the effect of variable density is confined to the body force term of the momentum equations, otherwise the thermodynamic and transport properties of the fluid are constant.
2. The two-phase fluid mixture is assumed to be incompressible.
3. The fluid is Newtonian.
4. The flow is laminar and two dimensional.

The governing hydrodynamic equations are as follows

$$\frac{\partial u}{\partial x} + \frac{\partial v}{\partial y} = 0 \quad [18]$$

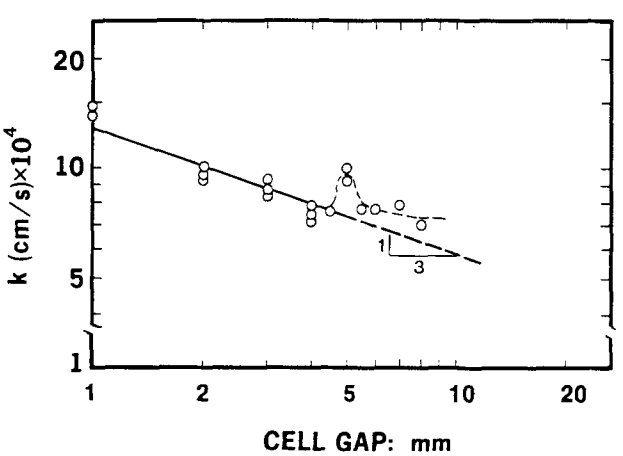

Fig. 9. Mass-transfer coefficient *vs.* cell gap isolated bubble-induced convection.

$$\rho_L\left(u\frac{\partial u}{\partial x} + v\frac{\partial u}{\partial y}\right) = -\frac{\partial p}{\partial x} - \rho g + \mu\left(\frac{\partial^2 u}{\partial x^2} + \frac{\partial^2 u}{\partial y^2}\right) \quad [19]$$

$$\rho_L\left(u\frac{\partial v}{\partial x} + v\frac{\partial v}{\partial y}\right) = -\frac{\partial p}{\partial x} + \mu\left(\frac{\partial^2 v}{\partial x^2} + \frac{\partial^2 v}{\partial y^2}\right) \quad [20]$$

Equation [18] is the continuity equation and Eq. [19] and [20] are the Navier-Stokes equations in x and y directions, respectively. The density in the gravity term of Eq. [19] is given by

$$\rho = \frac{\rho_L V_L + \rho_g V_g}{V_T}$$

Substituting

$$\epsilon = \frac{V_g}{V_T}$$

$$\rho = \rho_L\left(1 - \epsilon + \frac{\rho_g}{\rho_L}\epsilon\right)$$

The ratio of ρ_g/ρ_L is generally very small and hence the last term may be neglected

$$\rho = \rho_L(1 - \epsilon) \quad [21]$$

The density ρ, in the gravity term of Eq. [19] can be replaced by Eq. [21].

Now we have a system of three simultaneous nonlinear second-order partial differential equations involving four unknowns: u, v, p, and ϵ. A fourth equation which relates the concentration of the bubbles or the void fraction distribution in the x-y plane to the velocity components, pressure, and the physical properties of the two phases is required in order to be able to solve these equations. Various assumptions for the void fraction distribution are presented in the next section as a mathematical expression for this function is unknown and an analysis from first principles is complicated. However, qualitative information on the behavior of this function is available. Recently, Ziegler and Evans (15) used a convective diffusion equation to describe this function under turbulent flow, however, as far as we know, there has not been any investigation in support of their assumption. Furthermore, the bubble turbulent diffusivity, the bubble diameter, and the relative velocity are needed for solving the convective diffusion of the bubbles.

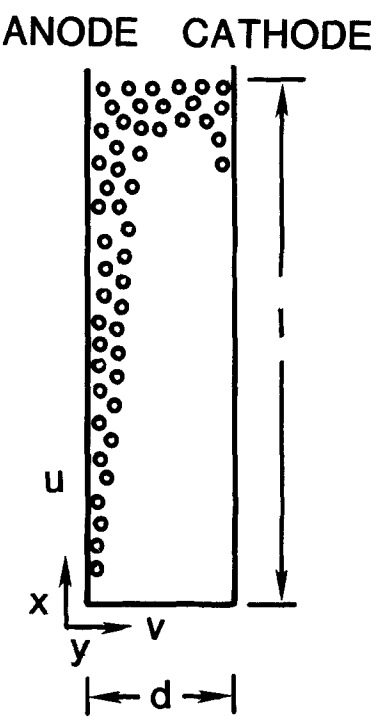

Fig. 10. The schematics of electrochemical cell with coordinate system.

Downloaded on 2015-06-09 to IP 141.210.2.78 address. Redistribution subject to ECS terms of use (see ecsdl.org/site/terms_use) unless CC License in place (see abstract).

The boundary conditions for the differential equations are

$$\begin{aligned} &y = 0 \text{ and } y = d && u = 0 && v = 0 \\ &x = 0 && u = 0 && v = 0 \\ &x = l && u = 0 && \frac{\partial v}{\partial x} = 0 \end{aligned} \qquad [22]$$

To obtain an approximate solution of the four equations one may proceed by the elimination of the pressure term from the momentum equations. Further, the continuity equation is satisfied by the introduction of a stream function ψ, defined as

$$u = \frac{\partial \psi}{\partial y} \qquad v = -\frac{\partial \psi}{\partial x}$$

This procedure leads to a fourth-order equation in terms of ψ. This formulation has been used by Rubel and Landis (24) for natural convection problem in a vertical rectangular enclosure.

The pressure terms from the two momentum equations are eliminated by appropriate differentiations and subtraction of Eq. [19] and [20]. The resulting equation, following simplification, can be written

$$u\frac{\partial^2 u}{\partial x \partial y} + v\frac{\partial^2 u}{\partial y^2} - u\frac{\partial^2 v}{\partial x^2} - v\frac{\partial^2 v}{\partial x \partial y} = g\frac{\partial \epsilon(x, y)}{\partial y} + \nu\frac{\partial}{\partial y}\nabla^2 u - \nu\frac{\partial}{\partial x}\nabla^2 v \qquad [23]$$

Equations [18] and [23] describe the fluid flow due to bubble-driven fluid circulation. Note that the pressure term has been eliminated, however, the order of the equations has increased from two to three.

The following dimensionless variables are introduced into Eq. [18] and [23]

$$U = \frac{ud}{\nu} \qquad V = \frac{vd}{\nu}$$

$$X = \frac{x}{d} \qquad Y = \frac{y}{d} \qquad [24]$$

The following equations in terms of the dimensionless variables are obtained

$$\frac{\partial U}{\partial X} + \frac{\partial V}{\partial Y} = 0 \qquad [25]$$

$$U\frac{\partial^2 U}{\partial X \partial Y} + V\frac{\partial^2 U}{\partial Y^2} - U\frac{\partial^2 V}{\partial X^2} - V\frac{\partial^2 V}{\partial X \partial Y} = \frac{gd^3}{\nu^2}\frac{\partial \epsilon(X, Y)}{\partial Y} + \frac{\partial}{\partial Y}\nabla^2 U - \frac{\partial}{\partial X}\nabla^2 V \qquad [26]$$

A dimensionless stream function defined by the following equations is introduced

$$U = \frac{\partial \psi}{\partial Y}$$

$$V = -\frac{\partial \psi}{\partial X} \qquad [27]$$

Notice that the stream function is defined in such a way that it satisfies the continuity equation, Eq. [25]. Equation [26], in terms of stream function, is given by Eq. [28]

$$\frac{\partial \psi}{\partial Y}\frac{\partial}{\partial X}\left(\frac{\partial^2 \psi}{\partial X^2} + \frac{\partial^2 \psi}{\partial Y^2}\right) - \frac{\partial \psi}{\partial X}\frac{\partial}{\partial Y}\left(\frac{\partial^2 \psi}{\partial X^2} + \frac{\partial^2 \psi}{\partial Y^2}\right) = \frac{gd^3}{\nu^2}\frac{\partial \epsilon(X, Y)}{\partial Y} + \nabla^2\left(\frac{\partial^2 \psi}{\partial X^2} + \frac{\partial^2 \psi}{\partial Y^2}\right) \qquad [28]$$

The dimensionless boundary conditions are as follows

$$\begin{aligned} &y = 0 \text{ and } Y = 1 && \psi = 0 && \frac{\partial \psi}{\partial Y} = 0 \\ &X = 0 && \psi = 0 && \frac{\partial \psi}{\partial Y} = 0 \\ &x = \frac{l}{d} && \psi = 0 && \frac{\partial^2 \psi}{\partial X^2} = 0 \end{aligned} \qquad [29]$$

The solution to Eq. [28], subjected to the boundary conditions in Eq. [29], would give a stream function field. The velocity components could be obtained from the stream function by differentiation according to Eq. [27].

The nonlinear fourth-order partial differential equation in terms of a stream function is solved using a generalized Newton's method described by Rubel and Landis (24). This implicit method of solution is stable and has a rapidly converging iteration scheme. A detailed description of the numerical method for solving the equation is given by Shah (17). All calculations were performed on a personal computer using an assembly language program. The effect of mesh size was studied by comparing the stream functions obtained by using different size grids. The more accurate values of the stream function is found by extrapolation of the stream function values obtained by the two finest grids. The results of this investigation are given in (17).

Assumption of void fraction distribution.—As discussed earlier, the void fraction distribution and stream function field are coupled, hence the stream functions obtained by numerical solution of the governing equation depends on the assumed void fraction distribution. Furthermore, among the infinite number of void fraction distributions that can be assumed to obtain the stream functions, only very few can physically exist in a real system. In the absence of a fundamental relation between void fraction and velocity field or stream function, the fictitious void fraction distributions are eliminated using the qualitative information available in literature and experimental observations (17). It is necessary to point out that this is only an approximate method through which a qualitative insight into the bubble driven fluid circulation can be gained.

It was experimentally observed that in a narrow vertical channel the bubbles are confined to a region near the vertical gas evolving wall and the boundary between the region containing gas bubbles and bubble-free region is sharp and distinct (17). The bubble envelope expands along the height of the column and may or may not reach the opposing wall depending on the cell gap, cell height, and rate of gas evolution. Typical shapes of the bubble envelope in vertical slots are shown and discussed in (17). The sudden expansion of the bubble envelope near the top of the cavity was experimentally observed.

A brief comment on the types of void fraction distributions primarily used in this study is in order. The types of void fraction distributions described here are thought to simulate the real void fraction distribution. In the very first numerical experiment the void fraction at the origin of the space coordinate (see Fig. 11) was assumed zero and was increased linearly along the gas evolving wall and decreased linearly to zero across the cell gap as shown in Fig. 11a. In this distribution none of the gas bubbles reach the opposite wall at $y = d$. In another simulation, a constant nonzero value of void fraction was assumed in the entire bubble envelope and a zero void fraction was assumed outside the bubble envelope as shown in Fig. 11b. The shape of the bubble envelope was also varied. In yet another simulation a constant nonzero void fraction was assumed along the gas evolving vertical wall and the void fraction linearly decreased in the horizontal direction to zero along the boundary of the bubble envelope as shown in Fig. 11c. In this case also the shape of the bubble envelope was changed. A sudden expansion of the bubble envelope near the top of the channel, as shown in Fig. 11d, was also simulated.

Downloaded on 2015-06-09 to IP 141.210.2.78 address. Redistribution subject to ECS terms of use (see ecsdl.org/site/terms_use) unless CC License in place (see abstract).

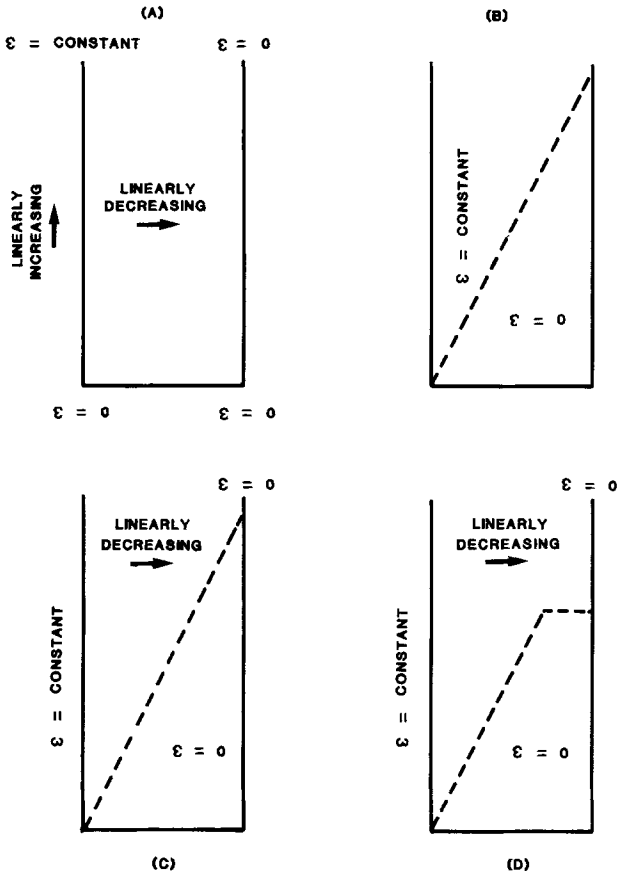

Fig. 11. Assumed void fraction distributions

Results and Discussion

The results of the numerical study are presented in the form of stream function contours. All contours were obtained by linear interpolation of the nodal point values. For improved clarity of presentation, only a few stream function contours are included. The value of the stream function at a point is proportional to the flow per unit time crossing any line joining the point to the wall. Due to the uncertainty associated with the assumption of the final steady-state void fraction distribution, the analysis and comparison of the results presented here must remain qualitative in nature.

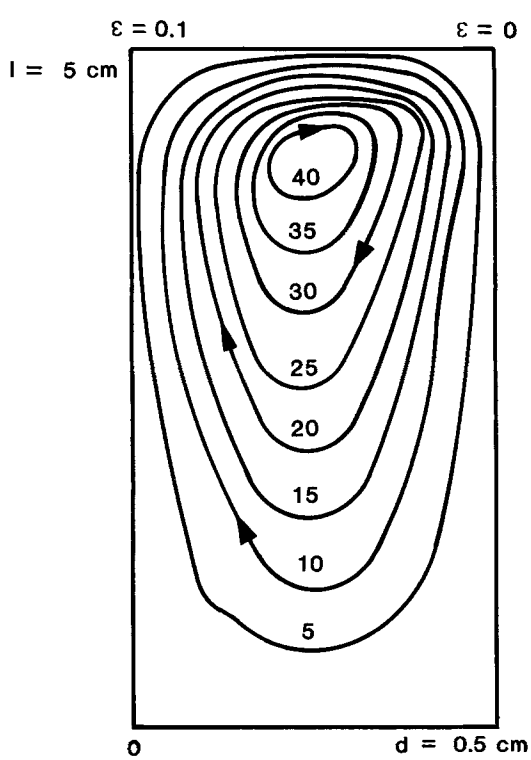

Fig. 12. Streamlines for void fraction distribution as shown in Fig. 11a, cell gap d = 0.5 cm and height l = 5 cm.

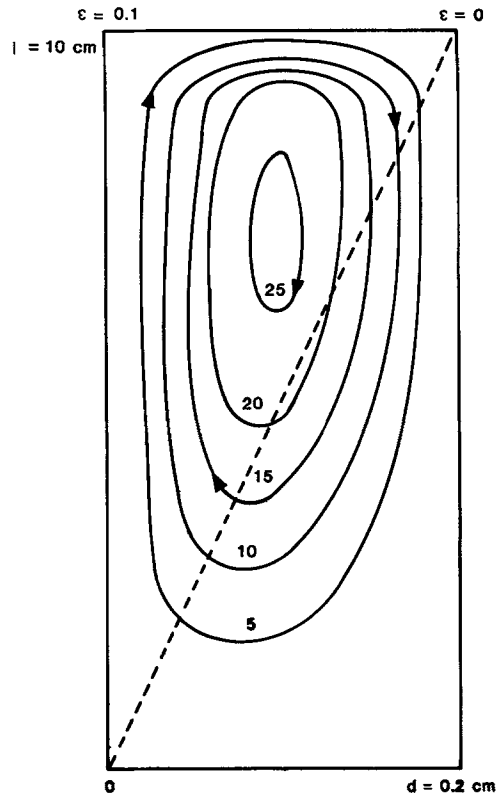

Fig. 13. Streamlines for void fraction distribution as shown in Fig. 11c, cell gap d = 0.2 cm and height l = 10 cm.

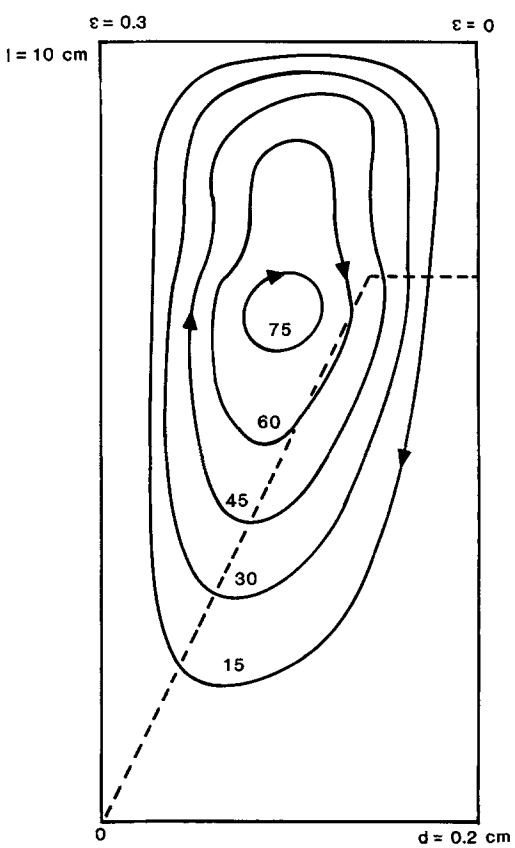

Fig. 14. Streamlines for void fraction distribution as shown in Fig. 11d, cell gap d = 0.2 cm and height l = 10 cm.

Downloaded on 2015-06-09 to IP 141.210.2.78 address. Redistribution subject to ECS terms of use (see ecsdl.org/site/terms_use) unless CC License in place (see abstract).

Figure 12 shows the stream function distribution for the cell gap of 0.5 cm and height of 5 cm. This distribution was obtained using void fraction distribution shown in Fig. 11a. The closeness of the stream lines at the top indicates a higher velocity in the horizontal direction. This is in agreement with the experimental observation (17) of intense circulation of electrolyte at the top of the cavity as shown in Fig. 5. This unicellular flow pattern is similar to one reported by Rubel and Landis (24) for natural convection with moderate Rayleigh numbers ($<10^5$). Figure 13 shows a similar stream function distribution for the cell gap of 0.2 cm and height of 10 cm. A dashed line indicates the boundary of the bubble envelope. The void fraction distribution used for obtaining this contour was similar to the one shown in Fig. 11c. A constant void fraction of 0.1 was assumed along the gas evolving electrode (the left-hand vertical border). Once again the closeness of the stream lines near the top of the cavity indicates a higher horizontal velocity. The stream function distribution in Fig. 14 is for a cell with the same parameters as in Fig. 13 except for the shape of the bubble envelope and constant void fraction of 0.3 along the gas evolving electrode. Comparison of Fig. 14 with Fig. 13 shows that the flow patterns in the two cases are similar. However the shape of the stream lines slightly above the eye of the loop in Fig. 14 indicates the possibility of a second circulation loop. It should be noticed that in Fig. 14 the stream function values are approximately three times that of the stream function values in Fig. 13. This increase in stream function is due to the threefold increase in the void fraction at the gas evolving wall. A similar proportionate increase in the stream function was observed in many other numerical experiments. A higher stream function value indicates more intense liquid circulation. The stream lines in Fig. 15 are for a cell with the same parameters as in Fig. 13, except for a change in cell gap from 0.2 to 0.3 cm. The higher value of stream function for larger cell gap indicates more intense circulation and is due to decrease in the viscous losses. The effect of decrease in the viscous losses with increasing cell gap can be clearly noticed in Fig. 16, where the stream lines for a cell gap of 0.5 cm are shown. The distinctive feature in the stream lines in Fig. 16 is the presence of two circulation loops. Multicellular flow patterns in a narrow cavity have been reported in the literature. Elder (25) experimentally observed a multicellular flow due to natural convection in a cavity with open top. He noticed the appearance of strong cells at Rayleigh number greater than 10^5 and noted that the size of these cells decreased while their number increased with an increase in the Rayleigh number. The multicellular flow in the case of natural convection due to temperature gradient has been numerically predicted by De Vahl Davis (26), Wilkes and Churchill (27), and Pepper and Harris (28). De Vahl Davis (26) noted that at high Rayleigh numbers the strong vorticity is able to sustain flow in opposite directions, similar to the one seen in Fig. 16. The second circulation loop in Fig. 16 causes an intense mixing of electrolyte at the top and an increased rate of mass transfer there. Both of these effects were experimentally observed in a zinc-chlorine cell (17-19).

Conclusions

The bubble-induced convection in a vertical thin slot is isolated from other modes of convection using a composite electrode. The composite electrode, 10 cm high, is made of a porous layer of titanium, plasma sprayed on a porous graphite substrate. The average rate of mass transfer generally decreases with increasing cell gap, except at around a cell gap of 0.5 cm where a local maximum is observed. Two independent mechanisms of mass transfer contribute to the overall rate of mass transfer. The two mechanisms are circulation of liquid due to nonuniform distribution of bubbles and stirring caused by the rising bubbles. The local rate of mass transfer increases with height and decreases as the cell gap increases to 0.3 cm. With further increase in the cell gap the local rate of mass transfer coefficient increases, in agreement with the observed local maximum in the average rate of mass transfer. Mass transfer under bubble-induced convection can be treated as a turbulent natural convection.

A mathematical model for bubble-driven fluid flow in an electrochemical cell is presented. The cell consists of a narrow vertical slot where gas evolves electrochemically at one wall. The bottom of the cell is closed and the top is a free surface. The numerical results indicate the presence

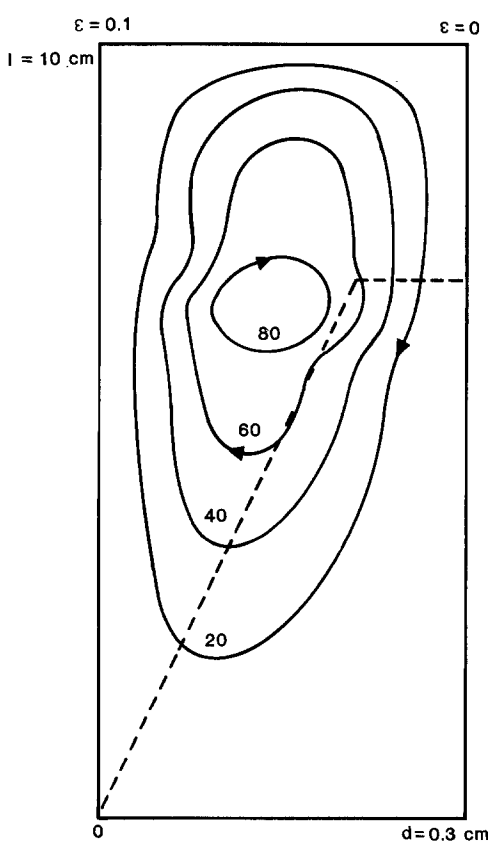

Fig. 15. Streamlines for void fraction distribution as shown in Fig. 2d, cell gap d = 0.3 cm and height l = 10 cm.

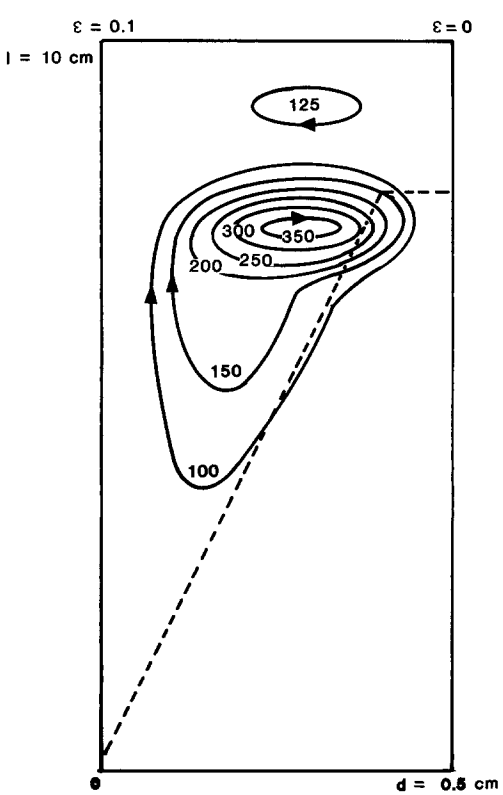

Fig. 16. Streamlines for void fraction distribution as shown in Fig. 2d, cell gap d = 0.5 cm and height l = 10 cm.

Downloaded on 2015-06-09 to IP 141.210.2.78 address. Redistribution subject to ECS terms of use (see ecsdl.org/site/terms_use) unless CC License in place (see abstract).

of circulatory flow which depends strongly on the cell gap, height, and assumed void fraction. The shape of the bubble envelope and the distribution of the void fraction determine the intensity of the circulation and the possibility of multicellular flow patterns.

Acknowledgment

This work was jointly supported by Energy Development Associates and the Electric Power Research Institute.

Manuscript submitted Nov. 2, 1987; revised manuscript received March 25, 1988.

REFERENCES

1. L. J. J. Janssen, *J. Appl. Electrochem.*, **17,** 1177 (1987).
2. H. Vogt, in "Comprehensive Treatise of Electrochemistry," E. Yeager, J. O'M. Bockris, B. E. Conway and S. Sarangapani, Editors, Plenum Press, New York and London (1983).
3. N. Ibl and J. Venczel, *Metalloberfaeche,* **24,** 365 (1970).
4. N. Ibl. *Chem. Ingr.-Tech.*, **35,** 353 (1963).
5. J. Venczel, *Electrochim. Acta,* **15,** 1909 (1970).
6. N. Ibl, E. Adam, J. Venczel, and E. Schlach, *Chem.-Ingr.-Tech.*, **43,** 202 (1971).
7. A. S. Gendron and V. A. Ettel, *Can. J. Chem. Eng.*, **53,** 36 (1973).
8. V. A. Ettel, B. V. Tilak, and A. S. Gendron, *This Journal,* **121,** 876 (1974).
9. S. Mohanta and T. Z. Fahidy, *J. Appl. Electrochem.*, **7,** 235 (1977).
10. G. H. Sedahmed, *ibid.*, **10,** 351 (1980).
11. G. H. Sedahmed and L. W. Shemilt, *ibid.*, **11,** 537 (1981).
12. L. Sigrist, O. Dossenbach, and N. Ibl, *Int. J. Heat Mass Transfer,* **22,** 1393 (1979).
13. N. Ibl, *Electrochim. Acta,* **24,** 1105 (1979).
14. D. N. Cavatorta and U. Böhm, *J. Appl. Electrochem.*, **17,** 340 (1987).
15. D. Ziegler and J. W. Evans, *This Journal,* **133,** 567 (1986).
16. J. T. Kim and J. Jorne, *ibid.*, **125,** 89 (1978).
17. A. Shah, Ph.D. Dissertation, Wayne State University, Detroit, MI (1986).
18. Electric Power Research Institute, EM-1414, (May 1980).
19. Electric Power Research Institute, EM-3136, (June 1983).
20. N. Zuber, *Int. J. Heat Mass Transfer,* **6,** 53 (1963).
21. L. J. J. Janssen and J. G. Hoogland, *Electrochim. Acta,* **15,** 1013 (1970); **18,** 543 (1973).
22. L. J. J. Janssen and E. Barendrecht, *ibid.*, **24,** 693 (1979).
23. M. G. Fouad and N. Ibl, *ibid.*, **3,** 233 (1960).
24. A. Rubel and F. Landis, The Physics of Fluids Supplement II, Page II-208 (1969).
25. J. W. Elder, *J. Fluid Mech.*, **23,** 77 (1965).
26. G. De Vahl Davis, *Int. J. Heat Mass Transfer,* **11,** 1675 (1968).
27. J. O. Wilkes and S. W. Churchill, *AIChE J.*, **12,** 161 (1966).
28. D. W. Pepper and S. D. Harris, *J. Fluids Eng.*, 650 (1977).

Mass Transfer under Combined Gas Evolution and Forced Convection

Atul Shah*,[1]

Department of Chemical Engineering, Wayne State University, Detroit, Michigan 48202

Jacob Jorne*

Department of Chemical Engineering, University of Rochester, Rochester, New York 14627

ABSTRACT

The combined effect of forced convection and bubble-induced convection on mass transfer in an electrochemical cell with vertical planar electrodes is investigated experimentally. The results indicate that a minimum is established in the mass-transfer coefficient due to the opposing effects of the two convections. A linear correlation exists between the rate of gas evolution and the rate of liquid flow at the minimum points. The effect of the cell gap is nonlinear, and it appears that a $-1/3$ power dependence exists. Beyond the point of minimum, the mass-transfer coefficient is dominated by the bubble-induced convection and a universal correlation exists between the rate of gas evolution and the increase in mass-transfer coefficient beyond the minimum value.

In many electrochemical processes gas evolution and forced convection interact to establish the mechanism for convective diffusion in the cell gap and near the electrode surface. Gas evolution can occur in two ways: external introduction of gas by bubbling gas through a porous medium and electrochemical gas evolution. Furthermore, the electrochemical gas evolution can occur at the electrode which is mass-transfer-limited or at an auxiliary or a counterelectrode. The present work is concerned with the situation in which gas evolution occurs at an auxiliary porous electrode and the induced electrolyte flow interacts with a forced convection through the porous electrode. This situation occurs for example in flow batteries (1), where porous electrodes are widely utilized and in electrochemical reactors where gas evolution occurs. In the zinc-chlorine battery (2, 3), for example, during charge, the chlorine-saturated zinc chloride electrolyte is circulated through the gas-evolving porous chlorine electrode. The combined flow affects the convective diffusion of dissolved chlorine to the zinc electrode, which is responsible for the coulombic inefficiency. In order to increase the coulombic efficiency of the zinc-chlorine battery, the convective diffusion of dissolved chlorine to the zinc electrode must be minimized. This can be achieved by balancing the forced convection by the opposing bubble-induced convection (1-3). In the chlor-alkali cell, gas evolution and flow of electrolyte interact to establish the flow pattern in the gaps between the electrodes and the separator (or membrane).

In the present work, the effect of bubble-induced convection and forced convection on the mass transfer within a vertical electrochemical cell is investigated. The experimental system is based on the design of the zinc-chlorine battery where chlorine gas is electrochemically evolved on a flow-through porous graphite electrode. The mass transport of dissolved chlorine to a parallel nearby zinc electrode is measured under various combinations of forced flow and gas evolution. The mass-transfer rate is measured by the limiting current method, although special precaution and arrangement had to be made in order to elimi-

* Electrochemical Society Active Member.
[1] Present address: Teledyne Analytical Instruments, City of Industry, California 91748.

Downloaded on 2015-06-09 to IP 141.210.2.78 address. Redistribution subject to ECS terms of use (see ecsdl.org/site/terms_use) unless CC License in place (see abstract).